



**HAL**  
open science

## From tomographic images to mesoscopic modelling of triaxial behavior of concrete

Ewa Piotrowska, Yann Malecot, Philippe Maurice Marin, Cédric Poinard,  
Laurent Daudeville

► **To cite this version:**

Ewa Piotrowska, Yann Malecot, Philippe Maurice Marin, Cédric Poinard, Laurent Daudeville. From tomographic images to mesoscopic modelling of triaxial behavior of concrete. FraMCoS-8, 2013, Toledo, Spain. pp.1401-1410. hal-01998297

**HAL Id: hal-01998297**

**<https://hal.science/hal-01998297v1>**

Submitted on 18 Dec 2024

**HAL** is a multi-disciplinary open access archive for the deposit and dissemination of scientific research documents, whether they are published or not. The documents may come from teaching and research institutions in France or abroad, or from public or private research centers.

L'archive ouverte pluridisciplinaire **HAL**, est destinée au dépôt et à la diffusion de documents scientifiques de niveau recherche, publiés ou non, émanant des établissements d'enseignement et de recherche français ou étrangers, des laboratoires publics ou privés.



Distributed under a Creative Commons Attribution 4.0 International License

## FROM TOMOGRAPHIC IMAGES TO MESOSCOPIC MODELLING OF TRIAXIAL BEHAVIOR OF CONCRETE

E. PIOTROWSKA<sup>\*</sup>, Y. MALECOT<sup>\*</sup>, P. MARIN<sup>\*</sup>, C. POINARD<sup>\*</sup> AND L. DAUDEVILLE<sup>\*</sup>

<sup>\*</sup> UJF-Grenoble 1, Grenoble-INP, CNRS UMR 5521,  
3SRLab, Grenoble F-38041, France.  
Email: yann.malecot@ujf-grenoble.fr

**Key words:** Concrete behavior, Compressive triaxial tests, Mesoscopic modeling, Segmentation, X-ray tomography

**Abstract:** This paper focuses on the discrete modeling of triaxial behavior of concrete. The model developed for simulating the response of concrete specimens takes into account the heterogeneity at the mesoscopic scale. Behaviors of mortar, rock, and their interaction are identified a priori, by means of experimental tests on the mortar and the rock. The construction method of the discrete element assembly is based on the 3D segmentation of tomographic images. Such a method allows the modeling of concrete at the mesoscopic scale with an internal structure similar to the one of the concrete tested experimentally. The comparisons between numerical and experimental results show the model is capable to reproduce the triaxial behavior of concrete for confining pressure varying from 0 to 650 MPa.

### 1 INTRODUCTION

This paper concerns the concrete behavior under extreme loading situations (ballistic impacts, penetration). During such loadings, concrete material undergoes severe triaxial loading [1,2]. Several authors characterized the triaxial behavior of concrete by performing quasi-static tests [3,4], like Gabet et al. [5,6], they used a very high capacity triaxial press to analyze the triaxial behavior of concrete under very high confinement. All of these studies led to the same conclusions, the confinement improves the strength of concrete and influences the failure pattern. Vu et al. showed that the Water/Cement ratio of the fresh mixture, which governs the uniaxial behavior, has no influence under high confining pressure whereas the saturation ratio of the hardened concrete becomes a predominant parameter [7,8].

To build macroscopic models able to reproduce these experimental results, it is

necessary to improve the understanding of mechanisms leading to the failure of concrete under high triaxial loading. In a previous paper X-ray tomography and optical observation methods were used to reveal the modification of damage modes with the increase of confinement [9,10]. One of the main limitations of the studies is the impossibility to access the visualization of the internal structure of concrete during the loading. In order to improve the analysis of cracks patterns the multiphase modeling, that takes into account the heterogeneities of the material, can be a useful tool since it enables accessing the internal structure of concrete at any time of the numerical test. Recently, mesoscopic models have been developed in order to differentiate the elements corresponding to the mortar from the one of the biggest aggregates [11,12] and possibly to the interface between both constituents [13]. These models are capable of reproducing

concrete behavior for a more or less important range of experimental tests [14].

The aim of this paper is to present a mesoscopic modeling, using the principles of lattice models [15] and discrete element method [16], able to reproduce concrete behavior under severe triaxial loading. The originality of the paper comes from the predictive feature of the developed model on the one hand; the behavior of mortar, aggregates and their interaction being identified a priori or from experimental tests realized on the mortar and the rock. On the other hand, the numerical sample construction relies on the 3D segmentation of tomographic images of the concrete. Such a construction method enables to obtain a numerical specimen with an internal structure similar to the real one, which gives hope for future work in the possibility to compare experimental cracks patterns with numerical ones.

The first part of this paper will cover the construction method of the numerical specimen. The different steps allowing obtaining an assembly of spheres that represents the real mesostructure of the concrete will be detailed. Subsequently, the features of the model will be presented, i.e. the different types of interactions and the laws governing their behavior. Since concrete is modeled as large aggregates surrounded by mortar, the third part will be devoted to the macroscopic modeling of these two constituents in order to identify the constitutive parameters associated to the interactions mortar-mortar and aggregate-aggregate and aggregate-mortar. Finally, the ability of the model to reproduce the triaxial behavior of concrete will be shown.

## 2 CONSTRUCTION OF THE NUMERICAL CONCRETE SPECIMEN

The numerical concrete specimen corresponds to a cubic and heterogeneous assembly of spheres that interact with each other. The distribution of material throughout spheres of different sizes enables to work easily with contact interactions that mainly occur after failure of cohesive interactions.

This assembly is heterogeneous in the meaning that the spheres represent materials of two different natures: rock and mortar. In addition, the macropores are taken into account and represented by the absence of spheres. The construction of this sample is based on a three-step procedure: the segmentation of images representing the concrete mesostructure, the assemblage of spheres and the identification of the nature of spheres.

### 2.1 Segmentation of images representing concrete mesostructure

The R30A7 concrete material used in the X-ray tomographic observations has been extensively studied by Gabet et al. [5,6], Vu et al. [7,8], and Malecot et al. [17]. Segmentation is a process that consists in partitioning an image into multiple segments (set of pixels) sharing certain characteristics. For the purpose of this study, two segmentation methods have been developed and then applied to X-ray tomographic images (slices) of R30A7 concrete. The scan parameters were chosen to well represent the mesostructure on the slices. Consequently, the concrete can be seen as a triphasic material, constituted of mortar, aggregates and macropores (entrapped porosity). Figure 1 (a) exhibits one of the slices of a cylindrical specimen: the lowest gray levels (black) represent the pores, the highest ones the aggregates and those intermediate the mortar. Thus, the aim of these two segmentation methods is to isolate the mortar and aggregates in order to create a new concrete specimen in which the meso-constituents are well localized.

### Entrapped porosity segmentation

The entrapped porosity segmentation is detailed in the article of Poinard et al. [9]. The image processing used, called thresholding, consists in transforming a gray level image into a binary image through a threshold gray level. In our case, since there is an uncertainty on the threshold gray level, it has been identified in order to obtain a value of porosity corresponding to the entrapped porosity measured experimentally. Figure 1 (b) presents

the result of the thresholding step. In order to have an image constituted only of pores, it is then required to remove the background (Figure 1(c)). This porosity segmentation can be applied slice by slice or to a volume as well.

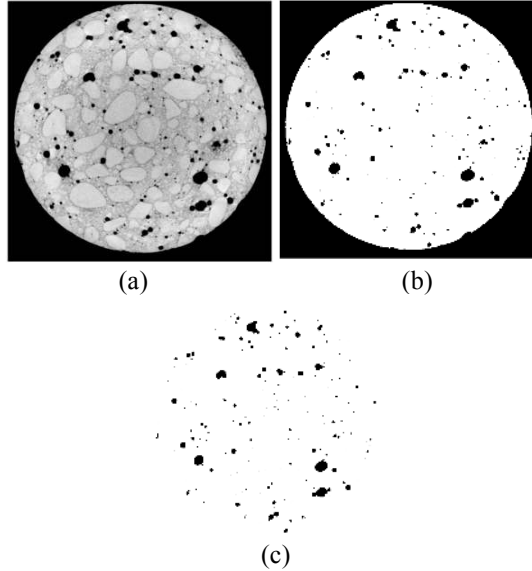


**Figure 1:** Step of porosity segmentation  
 (a) concrete slice obtained by Rx tomography  
 (b) after threshold processing  
 (c) after removing the background

### Aggregates segmentation

The segmentation of aggregates is more complicated to realize since the grey levels of both aggregates and mortar are partially mixed up. Nevertheless, on the slices representing the R30A7 concrete mesostructure, these two constituents exhibit a different feature, which is the homogeneity of the gray levels. Thus, the aggregates segmentation method is based on a “standard deviation” filter that enables to differentiate the gray levels of mortar from the ones of aggregates. Since the segmentation is applied to a set of slices, and so a volume, the standard deviation filter used is cubic. Its size has been chosen in order to obtain the best segmentation as possible. Figure 2 exhibits one of the slices of the cylindrical specimen before and after application of the standard deviation filter. It clearly appears, on both treated slices and associated gray level histogram, that the aggregates are now represented by gray levels higher than the ones of mortar (two peaks on the gray level

histogram), even if there is a small overlap. After the application of the standard deviation filter, a thresholding step allows to isolate the voxels corresponding to the aggregates. To do that, the threshold grey level is set to the minimal value between both peaks. Finally, simple modifications such as removing porosity are applied to obtain images representing only the large aggregates. Figure 3(a) exhibits a slice once the aggregates segmentation is done. Once the aggregates and porosity segmentations are done, they are combined to rebuild the concrete volume (Figure 3(b)).

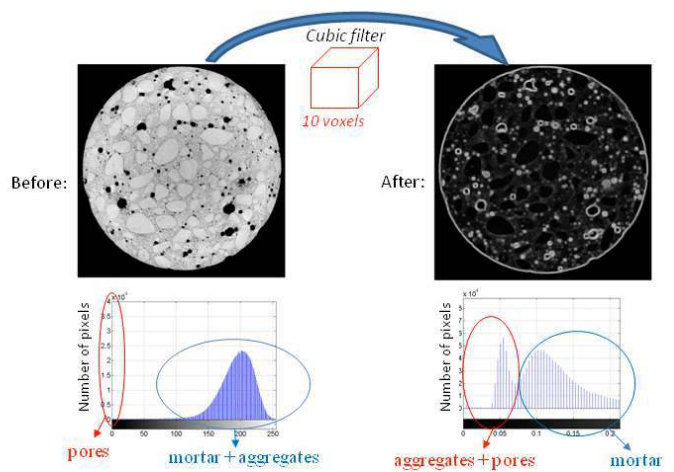


**Figure 2:** First steps of aggregates segmentation - application of the standard deviation filter

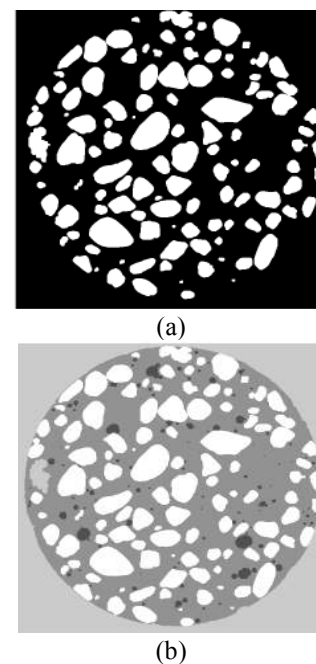


**Figure 3:** (a) Final result of aggregates segmentation (b) Combination of both aggregates and porosity segmentations

## 2.2 The spheres assembly construction

The spheres assembly construction is independent of what has been done in the previous section. This step starts by meshing a cube with tetrahedrons and continues by the application of an algorithm allowing obtaining an assembly of spheres. This algorithm described in Jerrier et al. [19], consists in filling each tetrahedron with spheres in the following way:

- at the center of each edge
- on the nodes
- on the triangular faces
- at the center of tetrahedron
- and in the void space

The interest of such a process is to provide an isotropic assembly of different size spheres assuring no orientation preference during failure. A cubic assembly of 9449 spheres was made for the purpose of this study.

## 2.3 Identification of the nature of spheres

The identification of the spheres nature consists in overlaying both cubes, the one segmented (section 2.1) and the one composed of spheres (section 2.2). The material is then assigned to each sphere depending on its position in the segmented cube. In addition, the spheres corresponding to the pores are removed out of the assembly what reduces the total number of spheres from 9449 to 9113. The Figure 4 exhibits the mesostructure of R30A7 concrete in both segmented cube and numerical specimen. For the assembly of spheres, visualization by Voronoï cells has been chosen with a representation of pores.

Table 1 presents the volume percentages of the different materials in a REV of concrete, in the segmented cube and in the numerical concrete sample of 9113 spheres. The proportions of the R30A7 meso-constituents are well preserved in the segmented cube and in the assembly of spheres. Nevertheless, it must be mentioned that even if the porosity percentages are very close, the number of pores in the numerical specimen is strongly reduced.

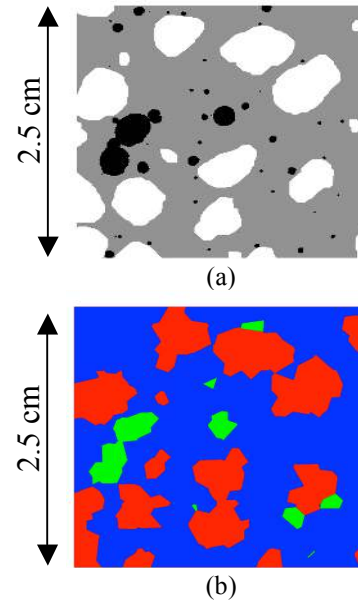


**Figure 4:** Mesostructure of a R30A7 concrete:  
 (a) in the segmented cube, black = pores, white = aggregates, grey = mortar  
 (b) in the assembly of 9449 Voronoï cells, green = pores, red = aggregates, blue = mortar

**Table 1:** Proportions of components of R30A7 mesostructure

	REV of concrete	Segmented cube	Assembly of 9113 spheres
Mortar (%)	59.5	63.4	62.8
Aggregates (%)	37	33.2	33.7
Entrapped porosity (%)	3.5	3.4	3.5

## 3 THE DISCRETE MODEL

The particularity of the proposed discrete method relies on the use of both the principle of the lattice model, in which the specimen is represented by network of beams, and the principle of the classical discrete element method, in which the material is represented by a collection of rigid spheres interacting by contacts. The combination of these two models enables reproducing the triaxial behavior of concrete up to very high confining pressures.

### 3.1 The interactions

Two kinds of interaction are distinguished in the model: the cohesive interactions (beam network) and the contacts. The cohesive interactions govern an important part of concrete behavior, particularly in the absence of the confinement. They are created at the beginning of the simulation, before any displacement, if the initial distance  $D_{init}$  between two spheres is sufficiently small (1). The interaction radius  $\lambda_{coh}$  is defined in order to obtain an average of 12 cohesive interactions by sphere, what assures a good reproducibility of the elastic features (Hentz et al. [18] and Rousseau et al. [20,21]). The cohesive interactions may break during simulation.

$$\lambda_{coh} \cdot (R_a + R_b) \geq D_{init} \quad (1)$$

where  $R_a$ ,  $R_b$ ,  $D_{init}$  are defined in Figure 5. The contact interactions are required to reproduce the behavior of concrete under high confinement. They occur during the simulation when two spheres, not linked by a cohesive interaction, get significantly closer. Actually, most of the contacts appear in place of cohesive interactions broken in traction, when the two spheres come back to the initial distance.

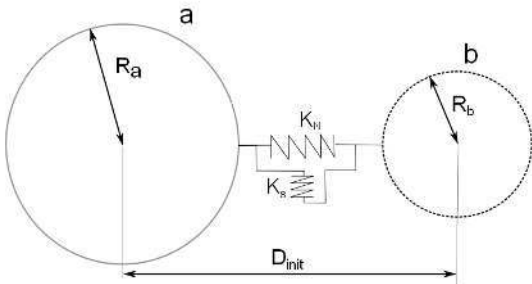


Figure 5: Features of an interaction

### 3.2 The behavior laws

This section presents briefly the behavior laws introduced at the interaction scale. The interaction force  $F$  representing the action of element  $a$  on element  $b$  (Figure 5) can be decomposed into a normal force  $F_N$  and a shear force  $F_S$ . Figure 6 presents the relation between the normal force and the distance  $D$  between the centers of the two spheres.

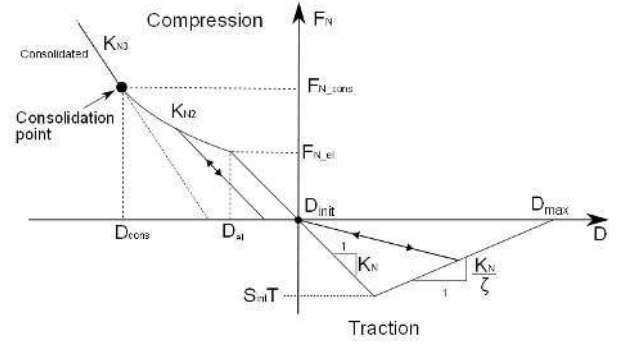


Figure 6: Normal behavior law of cohesive and contact interactions

The compressive behavior of interactions is similar to the one observed at the macroscopic scale for cement matrix materials during hydrostatic compression tests. It starts by a linear elastic phase governed by the stiffness  $K_N$  (2), what is followed by a compaction phase controlled by the non-linear stiffness  $K_{N2}$  (3). After the consolidation point, the behavior is linear elastic with a stiffness  $K_{N3} > K_N$  (4).

$$F_N = (D_{init} - D)K_N \quad (2)$$

$$F_N = (D_{init} - D_{el})K_N + (D_{el} - D)K_{N2} \quad (3)$$

$$F_N = (D_{init} - D_{el})K_N + (D_{el} - D_{cons})K_{N2} + (D_{cons} - D)K_{N3} \quad (4)$$

An elastic brittle law with damage governs the tensile behavior of cohesive interactions. The failure appears when the normal force exceeds the tensile strength and is more or less brittle depending on the value of the softening parameter  $\zeta$ .

The tangential behavior is governed by the tangential stiffness  $K_S$  (Figure 5) through the modified Mohr coulomb law (Figure 7). The limitation of the tangential force facilitates the tangential sliding and so the arrival of the failure of interactions. It must be noted that to take into account the elements size variation, the surface  $S_{int}$ , defined by  $\text{Min}(\pi R_a^2, \pi R_b^2)$  (Figure 5) is used.

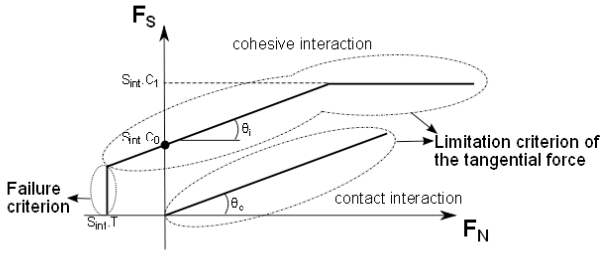


Figure 7: Modified Mohr Coulomb criterion

### 3.3 Strategy for modeling the concrete behavior at the mesoscopic scale

The behavior laws presented in the previous part are governed by numerous parameters that need to be identified. Since concrete is modeled as a heterogeneous material, these parameters depend on the nature of the interaction: mortar-mortar, mortar-aggregate, etc. The strategy consists of modeling mortar and rock as homogeneous materials in order to determine the parameters of interactions mortar-mortar and aggregate-aggregate. The following steps of the trial and error identification procedure are performed:

- Simple compression tests to identify the normal stiffness  $K_N$  and the tangential stiffness  $K_S$  that reproduce the elastic features  $E$ ,  $\nu$  of the material.
- Simple compression tests and tensile tests to identify  $T$ ,  $\zeta$  and  $C_0$  that reproduce as much as possible the pre and post peak behavior of the material.
- Hydrostatic compression tests to identify the nonlinear stiffness  $K_{N2}$
- Triaxial compression tests at different confining pressures to identify the parameters  $C_1$ ,  $\phi_i$  and  $\phi_c$ .

For the aggregate-mortar interaction, since we don't have any experimental tests, an a priori identification of the parameters is performed, what will be detailed in section 5.1.

## 4. MACROSCOPIC MODELING OF THE CONSTITUENTS EXISTING IN THE MESOSTRUCTURE OF CONCRETE

### 4.1 Mortar

This section shows the capability of the model to simulate the behavior of mortar

characterized experimentally by Dupray et al. [12]. Simple compression test presented in Figure 8 shows very good reproducibility of experimental results in terms of elastic parameters, limit states (stress peak and contractancy-dilatancy transition) and post peak behavior.

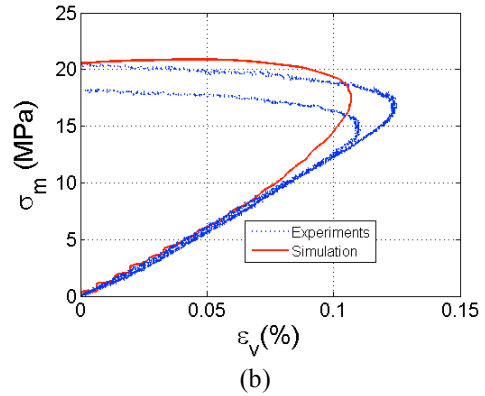
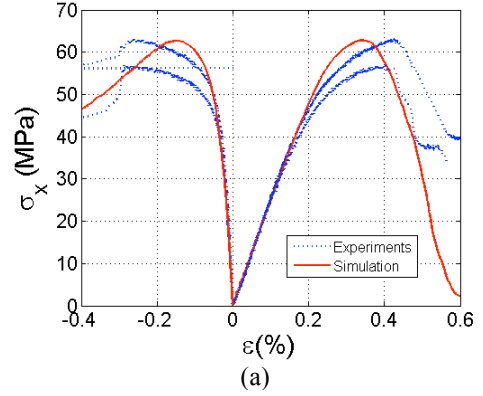
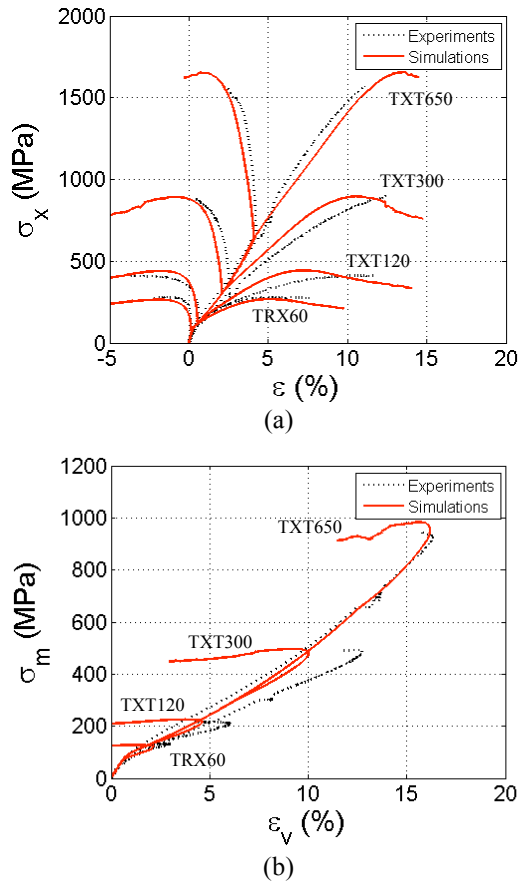


Figure 8: Uniaxial behavior of mortar  
(a) axial and transverse behavior  
(b) volumetric behavior

Figure 9 interests in the triaxial compression tests at different levels of confinement. The numerical sample reproduces in a remarkable way the behavior of mortar: not only are the contractancy-dilatancy transition reproduced, but also the shape of curves. The increase in ductility with the confining pressure found experimentally is also observed numerically. The stiffness of the numerical specimen is significantly lower than the one of the mortar at the early stages of deviatoric loading at high confinement. This difference can be largely explained by the creep existing at the beginning of the deviatoric part of the experimental test and not taken into account in the simulations.





**Figure 9:** Triaxial behavior of mortar  
 (a) axial and transverse behavior  
 (b) volumetric behavior

#### 4.2 Rock

The behavior of the quartzite sandstone existing in the form of aggregates in the R30A7 concrete has been characterized through experimental tests: uniaxial compression, triaxial compression at 50 MPa, hydrostatic compression and Brazilian test. Figure 10 shows the comparison between numerical and experimental results for three different compressive tests. We can observe that the elastic features, the stress peaks and the post peak behaviors are well reproduced by the model. Nevertheless it must be mentioned that it is not possible to satisfactorily reproduce the value of tensile strength determined from the Brazilian test (23 MPa) at the same time. It remains overestimated and equal to 40 MPa.

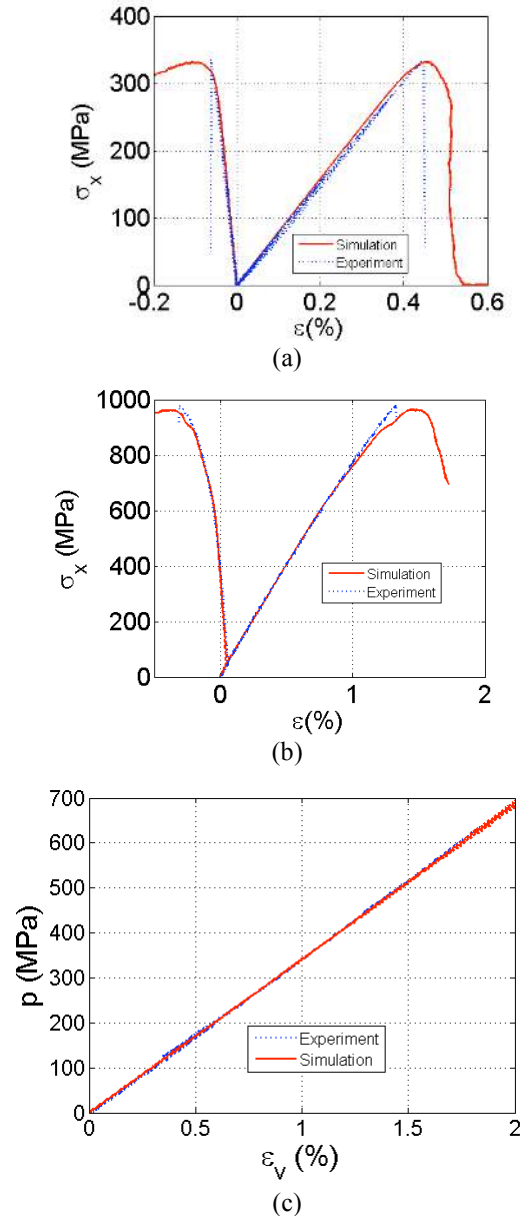


**Figure 10:** Behavior of a quartzite sandstone  
 (a) uniaxial compression  
 (b) triaxial compression at 50 MPa  
 (c) hydrostatic compression

### 5. MESOSCOPIC MODELING OF CONCRETE TRIAXIAL BEHAVIOR

The simulations presented in section 4 allowed to identify the parameters of mortar-mortar interaction and aggregate-aggregate interaction. Therefore, the parameters of two other types of interaction must be determined: mortar-aggregate and aggregate-aggregate (two different aggregates). The parameters governing aggregate-aggregate interaction were chosen equal to those of mortar-



aggregate interaction what is justified by their low percentage and the fact that a layer of mortar inevitably separates two aggregates.

### 5.1 Parameters identification of aggregate-mortar interaction

The parameters of the aggregate-mortar interaction are identified in an a priori manner due to the lack of experimental results. For the microscopic stiffnesses  $K_N$  and  $K_S$  governing the elastic behavior, the mean of the stiffnesses of rock and mortar are used. This choice is explained by the fact that the stiffness of an aggregate-mortar interaction can be seen as two stiffnesses in series, the one of mortar and the one of rock. Equation 5 presents the computation of the normal stiffness  $K_N$  defined by  $K_{N\_interface}$  for the aggregate-mortar interaction.

$$K_{N\_interface} = \frac{2(K_{N\_mortier} \cdot K_{N\_granulat})}{K_{N\_mortier} + K_{N\_granulat}} \quad (5)$$

Some authors showed that there exist the “Interfacial Transition Zone” between aggregates and cement paste that exhibits poor mechanical properties [22]. In order to take into account the weakness of this zone, the strength properties ( $T, C_0$ ) are chosen as mortar properties divided by the degradation coefficient, which is calibrated to reproduce the uniaxial strength. The other parameters of the aggregate-mortar interaction were chosen in order to obtain the best reproduction of the triaxial behavior of R30A7 concrete.

### 5.2 Behavior of the numerical concrete

Figures 11 et 12 shows the ability of the numerical concrete, defined as an heterogeneous assembly of spheres, to simulate the behavior of R30A7 concrete under compression tests more or less confined. The curves presented in Figure 11 show that the numerical concrete behaves in a quasi-identical manner with the real concrete during a uniaxial compressive test. The only difference concerns the post peak phase when the behavior is slightly less brittle numerically than experimentally.

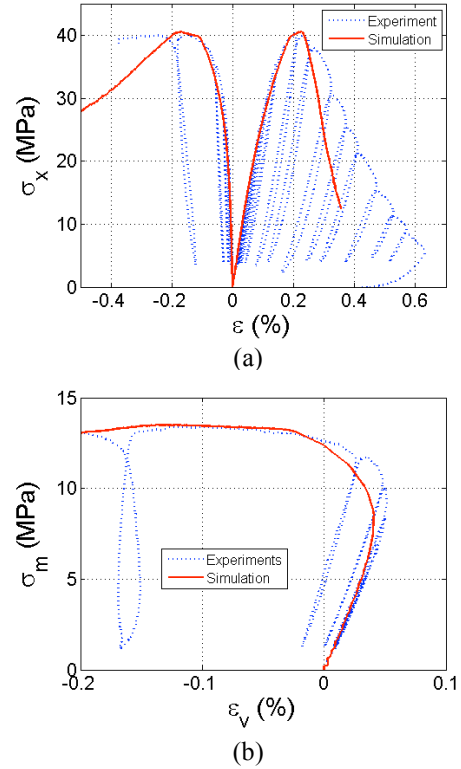


**Figure 11:** Uniaxial behavior of concrete  
(a) axial and transverse behavior  
(b) volumetric behavior

Figure 12 shows that the model is also efficient when simulating the triaxial compression tests at confinement ranging from 50 to 650 MPa. Indeed, the limit states (stress peak or plateau and contractancy-dilatancy transition) of the numerical and real concrete occur at comparable stress and strain levels, particularly for the low confinement. At the 650 MPa of confinement, the model slightly under estimates concrete strength.

## 12 CONCLUSIONS

A discrete model was used to reproduce the triaxial behavior of concrete. The model is realized at the mesoscopic scale, what means that the features of the three concrete mesostructure constituents: aggregates, mortar, pores, and their interaction are taken into account. In addition, in order to perform simulations on a numerical specimen similar to the real concrete, an original method of mesh conception based on the segmentation of tomographic images has been developed.

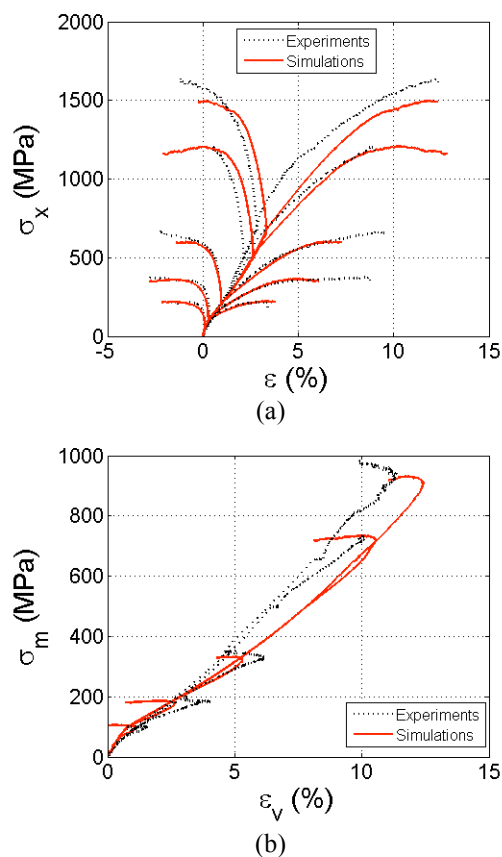


**Figure 12:** Triaxial behavior of concrete  
 (a) axial and transverse behavior  
 (b) volumetric behavior

The comparison between behavior curves coming from simulations and experimental tests showed the model is capable to reproduce the concrete response under triaxial loading more or less confined. Nevertheless, a macroscopic modeling, that is simpler, would be as much efficient. Besides, it was used to reproduce the behavior of mortar.

This mesoscopic modeling method is thus developed in order to improve the understanding of mechanisms leading to the failure of concrete subjected to high triaxial loadings, on one hand. Besides, work on the damage visualization is being developed in order to assess the model ability to reproduce the mechanisms observed experimentally. On the other hand, such a model, if it is enough consistent, might progressively replace the experimental tests to study the influence of the concrete mesostructure (aggregates size, aggregates volume/mortar volume, macroporosity, etc.) on the triaxial behavior.

## ACKNOWLEDGMENTS

The GIGA press has been installed in the 3SR Laboratory within the scope of a cooperative agreement signed with the French Defense Ministry's Armament Division. This research has been performed with the financial support of the Gramat Research Center (CEA ramat). We would like to thank Dr. Eric Buzaud (CEG) and Dr. Christophe Pontiroli for giving technical and scientific advice.

## REFERENCES

- [1] Zukas, J.A. Penetration and perforation of solids. *Impact Dynamics*. Krieger Publishing Company (1992).
- [2] Gran, J.K. and Frew, D.J. In-target radial stress measurements from penetration experiments into concrete by ogive-nose steel projectiles. *International Journal of Impact Engineering* (1997) **19**:715-726.
- [3] Schmidt, M.J. Cazacu, O. Green, M.L. Experimental and theoretical investigation of the high-pressure behavior of concrete. *International Journal for Numerical and Analytical Methods in Geomechanics* (2009) **33**:1-23.
- [4] Sfer, D. Carol, I. Gettu, R. and Etse, G. Study of the behaviour of concrete under triaxial compression. *Journal of Engineering Mechanics* (2002) **128**:156-163
- [5] Gabet, T. Malecot, Y. Daudeville, L. Triaxial behavior of concrete under high stresses: Influence of the loading path on compaction and limit states. *Cement and Concrete Research* (2008) **38**:403-412.
- [6] Gabet T., Vu X.H., Malecot Y. & Daudeville L. A new experimental technique for the analysis of concrete under high triaxial loading. *Journal de Physique IV* (2006) **134**:635-640.
- [7] Vu, X.H. Malecot, Y. Daudeville, L. and Buzaud, E. Effect of the water/cement ratio on concrete behavior under extreme loading, *Int J Numer Anal Methods Geomech* (2009) **33**:1867-1888.

- [8] Vu X.H., Malecot Y., Daudeville L. & Buzaud E. Experimental analysis of concrete behavior under high confinement: Effect of the saturation ratio. *International Journal of Solids and Structures* (2009) **46**(5):1105-1120.
- [9] Poinard, C. Malécot, Y. Daudeville, L. and Landis, E.N. Compression triaxial behavior of concrete: The role of the mesostructure by analysis of x-ray tomographic images. *EJECE* (2011) (in Press).
- [10] Poinard C., Malécot Y. and Daudeville L. Damage of concrete in a very high stress state: Experimental investigation. *Materials and Structures* (2010) **43**(1-2): 15–29.
- [11] La Borderie, C., Lawrence, C. and Menou, A. Approche mésoscopique du comportement du béton: Apport de la représentation géométrique. *REGC* (2007) **11**:407-421.
- [12] Dupray, F. Malecot, Y. Daudeville, L. and Buzaud, E. A mesoscopic model for the behavior of concrete under high confinement. *International Journal for Numerical and Analytical Methods in Geomechanics* (2009) **33**:1407-1423.
- [13] Lilliu, G. and Van Mier, J. G. M. On the relative use of micro-mechanical lattice analysis of 3-phase particule composites. *Engineering Fracture Mechanics* (2007) **74**:1174-1189.
- [14] Cusatis, G. Pelessone, D. Mencarelli A. and Baylot, J. Lattice Discrete Particle Model for failure behavior of concrete II. *Cement and Concrete Composites* (2011) **33**(9): 891–905.
- [15] Schlangen, E. et Van Mier, J. G. M. Experimental and numerical analysis of micromechanism of fracture of cement-based composites. *Cement and Concrete Composites*. (1992) **14**:105-108.
- [16] Cundall, P. A. and Strack, O. D. L. A discrete numerical model for granular assemblies. *Géotechnique* (1979) **29**:47-65.
- [17] Malecot, Y. Daudeville, L. Dupray, F. Poinard, C. and Buzaud, E. Strength and damage of concrete under high triaxial loading. *European Journal of Environmental and Civil Engineering* (2010) **14**:777-803.
- [18] Hentz S., Daudeville L., Donze F. Identification and validation of a discrete element model for concrete. *Journal of Engineering Mechanics* (2004) **130**(6): 709-719.
- [19] Jerier, J.F. Imbault, D. Donze, F.V. and Doremus, P. A geometric algorithm based on tetrahedral meshes to generate a dense polydisperse sphere packing. *Granular Matter*. (2009) **11**:43-52.
- [20] Rousseau J., Frangin E., Marin P. & Daudeville L. Damage prediction in the vicinity of an impact on a concrete structure: a combined FEM/DEM approach. *Computers and Concrete* (2008) **5**(4): 343-358.
- [21] Rousseau J., Frangin E., Marin P. & Daudeville L. Multidomain finite and discrete elements method for impact analysis of a concrete structure. *Engineering Structures* (2009) **31**(11): 2735-2743
- [22] Diamond, S. and Huang, J. The ITZ in concrete - a different view based on image analysis and SEM observations. *Cement & Concrete Composites* (2001) **23**:179-188.